7

Micro Gas Turbines

Flavio Caresana[1], Gabriele Comodi[1],
Leonardo Pelagalli[1] and Sandro Vagni[2]
[1]*Dipartimento di Energetica – Università Politecnica delle Marche*
[2]*Università degli Studi e-Campus*
Italy

1. Introduction

Conventional gas turbines (GTs) range from a size of one or a few MWe to more than 350 MWe (GTW, 2009). Those at the small end of the range are commonly used in industrial applications, for mechanical or onsite electrical power production, while the larger ones are usually installed in large-scale electrical power plants, often in combined cycle plants, and are typically located far away from the consuming region.
In the future distributed energy systems based on small local power plants are likely to spread; since they lie close to the final users, they reduce electrical transport losses, and make thermal energy recovery profitable both in energy-related and in economic terms (Papermans et al., 2005; IEA, 2002). These benefits explain the increasing interest in small-size generation systems.
Recently, gas turbines < 1 MWe, defined as micro gas turbines (MGTs), have appeared on the market. MGTs are different from large GTs and cannot therefore be considered merely as their smaller versions. Their advantages as distributed energy systems lie in their low environmental impact in terms of pollutants and in their competitive operation and maintenance (O&M) costs. MGTs appear to be particularly well suited for service sector, household and small industrial applications (Macchi et al., 2005; Zogg et al., 2007).

2. The technology of Micro Gas Turbines

The small power size of MGTs entails implications that affect the whole structure. In particular the low gas mass flow rate is reflected in machine size and rotational speed: the smaller the former, the greater the latter. MGTs therefore differ significantly from GTs, mainly in (i) the type of turbomachines used; (ii) the presence of a regenerator; and (iii) the high rotational speed, which is independent of grid frequency. In fact unlike GTs, MGTs commonly use high-revving, single-stage radial turbomachines rather than multi-stage axial ones, to achieve greater compactness and low manufacturing costs. As a consequence of the high rotational speed, the electrical current is generated at high frequency and is then converted to the grid frequency value (50 or 60 Hz) by power electronics. The turbocompressor and turbine are usually fitted on the same shaft as the electrical generator, which also serves as the starting motor. Single-stage radial machines afford limited compression ratios and need a regenerative cycle to attain satisfactory electrical efficiency.

Therefore a regenerator is usually installed between the compressor and the combustion chamber. Figures 1 and 2 show, respectively, the layout and corresponding thermodynamic cycle of a typical cogeneration MGT.

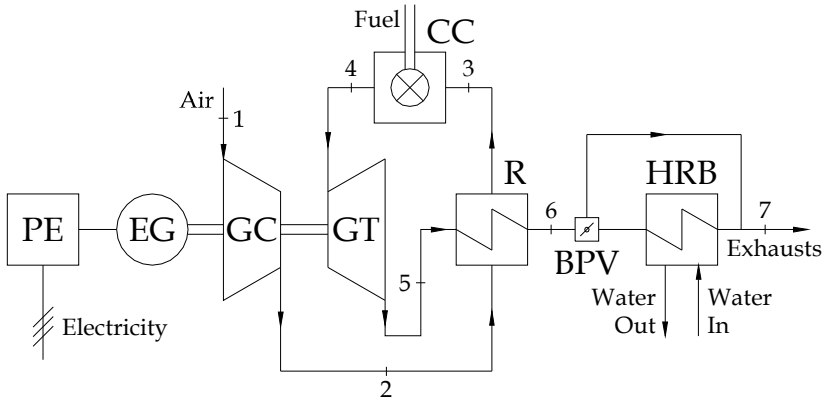

PE	Power Electronics	CC	Combustion Chamber
EG	Electrical Generator	R	Regenerator
GC	Gas Compressor	BPV	ByPass Valve
GT	Gas Turbine	HRB	Heat Recovery Boiler

Fig. 1. Layout of a typical cogeneration MGT

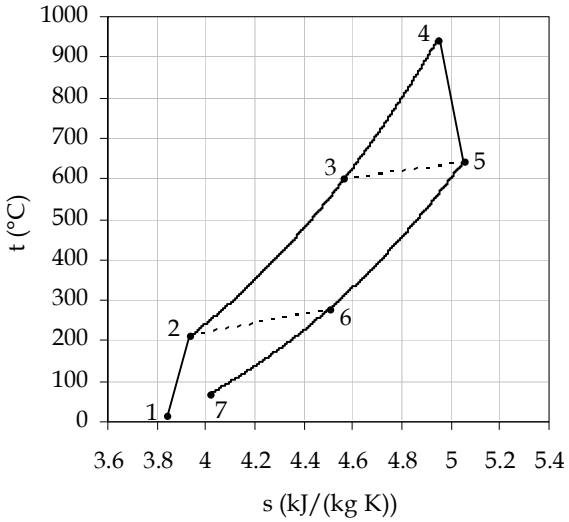

Fig. 2. MGT regenerative Brayton-Joule cycle

The ambient air (1, in both figures) is compressed by the centrifugal compressor; it then enters the regenerator (2), where it is preheated by the exhausts coming from the turbine, and is conveyed from the regenerator (3) to the combustion chamber, where it is used in the

combustion process to achieve the design turbine inlet temperature (4). The hot gases then expand through the turbine (5) and enter the regenerator. Given their fairly high temperature at the power unit exit (6), the exhausts can be sent to a heat recovery boiler (HRB), where they are used to heat water, before being discharged to the flue (7). In this configuration combined heat and power (CHP) production increases fuel energy conversion efficiency. When the thermal power demand is lower than the power that can be recovered from the exhausts, part of the fumes is conveyed directly to the chimney (7) via a bypass valve (BPV). The core power unit is fitted with auxiliary systems that include (i) fuel, (ii) lubrication, (iii) cooling, and (iv) control systems. The fuel feeding system compresses the fuel to the required injection pressure and regulates its flow to the combustion chamber according to the current operating condition. The lubrication system delivers oil to the rolling components, with the dual effect of reducing friction and removing heat. The cooling system keeps the operational temperatures of the different components, lubrication oil included, in the design ranges. The cooling fluid can be air, water, or both. The function of the electronic control system is to monitor MGT operation through continuous, real time checking of its main operational parameters.

3. Operation modes

MGTs can usually operate in two modes:

1. **Non-cogeneration** (electricity production only): the MGT provides the electrical power required by the user and all the available thermal power is discharged to the flue.
2. **Cogeneration** (combined production of electrical and thermal energy): the MGT produces the electrical and thermal power required by the user. MGTs operating in cogeneration mode can usually be set to work with electrical or with thermal power priority.
   a. *Electrical priority operating mode*
      In this operating mode the MGT produces the electrical power set by the user, while heat production is regulated by the BPV installed before the HRB. This is not an energy efficiency-optimized operating mode, because in conditions of high electrical and low thermal power demand a considerable amount of the recoverable heat is discharged to the flue.
   b. *Thermal priority operating mode*
      Thermal priority operation involves complete closure of the MGT bypass valve, so that all the exhaust gases from the regenerator pass through the HRB for thermal power recovery. Thermal power production is regulated by setting the electrical power. This mode maximizes MGT efficiency in all operating conditions.

4. Performance and emissions

The considerations made so far apply to most MGTs. The data presented below have been obtained from theoretical studies and experimental testing of a specific machine, a Turbec T100 PH (Turbec, 2002), which the authors have been using for their research work for several years (Caresana et al., 2006). With due caution, these findings can be extended to most MGTs. In this section, the performance and emissions of a real MGT-based plant are reported and some criticalities connected to MGT behaviour highlighted.
The main performance parameters of an MGT are:

- electrical power P_{el} ;
- thermal power P_{th} ;
- electrical efficiency η_{el} , defined as:

$$\eta_{el} = \frac{P_{el}}{\dot{m}_f LHV} \tag{1}$$

- thermal efficiency η_{th} , defined as:

$$\eta_{th} = \frac{P_{th}}{\dot{m}_f LHV} \tag{2}$$

- total efficiency η_{tot} , defined as:

$$\eta_{tot} = \frac{P_{el} + P_{th}}{\dot{m}_f LHV} = \eta_{el} + \eta_{th} \tag{3}$$

where $\dot{m}_f$ and LHV are the mass flow rate and the Lower Heating Value of the fuel, respectively.
Since electrical power is the main final output, we have represented the dependence of the other performance parameters on P_{el} (Figures 3-7). Unless specified otherwise, the experimental data refer to ISO ambient conditions, i.e. temperature and relative humidity (R.H.) equal to 15 °C and 60 % respectively (ISO, 1989).

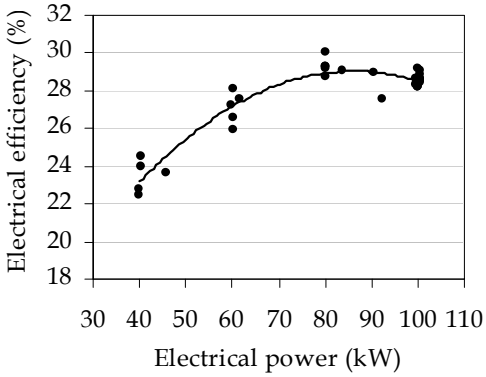

Fig. 3. Electrical efficiency

Figure 3 plots the trend of the electrical efficiency, which is consistently high from the nominal power down to a partial load of about 70 %, with a maximum slightly > 29 % around 80 kWe. Figures 4 and 5 report the thermal power and total efficiency data, respectively, for different degrees of BPV opening, calculated as the ratio between the thermal power recovered and that which can be recovered at the nominal power. The tests were conducted at a constant water flow rate of 2 l/s entering the HRB at a temperature of 50 °C.

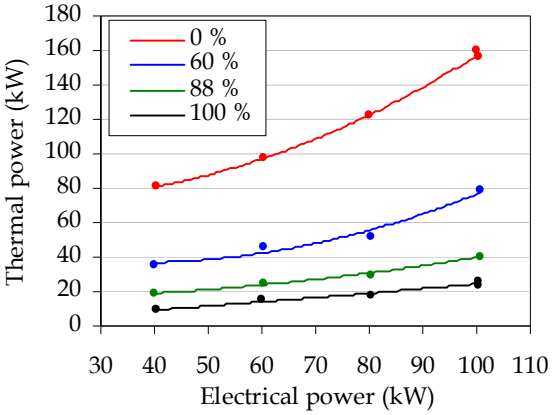

Fig. 4. Thermal power for different degrees of BPV opening

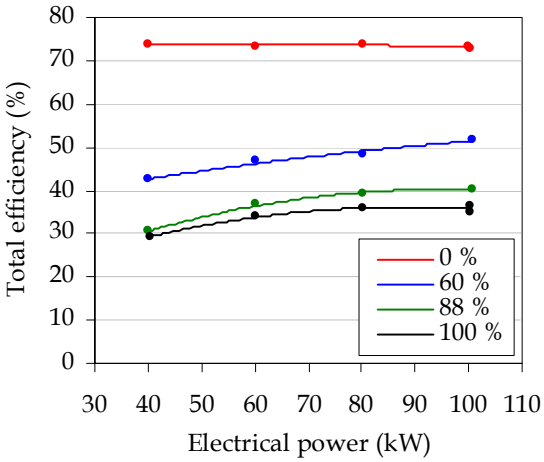

Fig. 5. Efficiencies for different degrees of BPV opening

As expected, greater BPV opening entailed a progressive reduction in the thermal power recovered, and consequently reduced total efficiency. This confirms that the thermal priority cogeneration mode maximizes fuel energy conversion efficiency. Figure 4 shows that a small part of the discharged thermal power is however transferred from the exhausts to the water, even with a completely open BPV. If this thermal power (about 25 kW at full load) is usefully recovered, total efficiency remains greater than electrical efficiency, as shown in Figure 5, otherwise total and electrical efficiencies necessarily coincide.

Figures 6 and 7 show the level of pollutants CO and NO_X, respectively. CO concentrations in the exhausts are low from 70 % to 100 % of the load, but they rise steeply with lower loads. The NO_X concentration is very low in all working conditions.

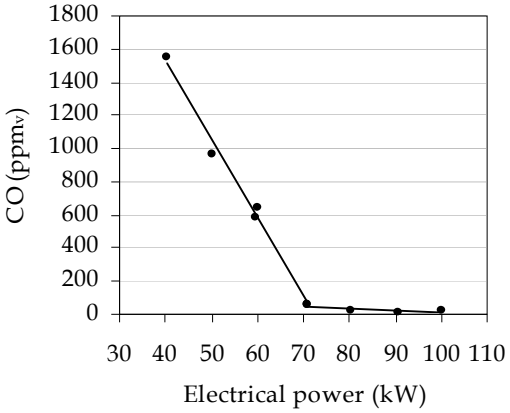

Fig. 6. CO concentration @ 15 % O_2

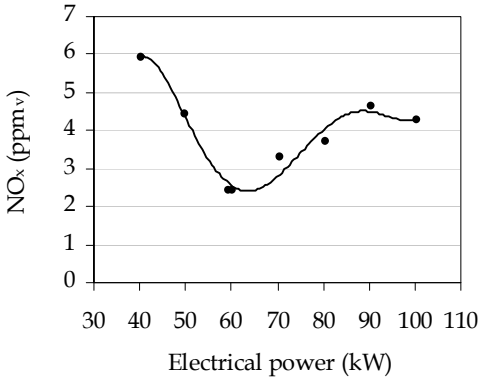

Fig. 7. NO_X concentration @ 15 % O_2

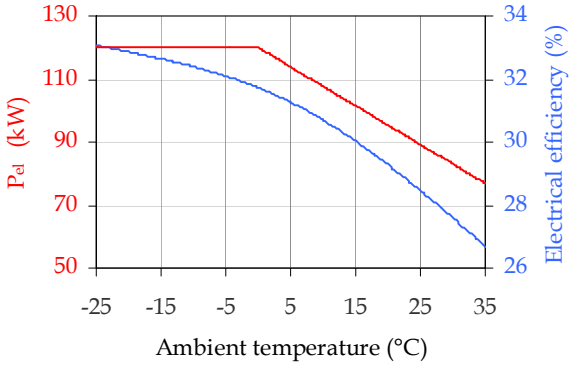

Fig. 8. Electrical performance vs ambient temperature

4.1 Influence of ambient parameters

The performance of MGTs, like those of GTs, are strongly affected by ambient conditions, particularly temperature. Figure 8 shows the values of nominal electrical power and efficiency as a function of the ambient temperature. In the T100 PH machine, electrical power generation at temperatures < 0 °C is limited electronically, to avoid overworking the machine. The decline observed at higher temperatures is explained by the lower air density and consequently lower mass flow rate through the power unit. A parallel decrease in electrical efficiency can also be noted.

4.2 Influence of heat recovery

The performance of a cogeneration system can be evaluated by comparison with the separate production of heat and electricity. The most commonly used index is the Primary Energy Saving (*PES*) index which, as the name suggests, quantifies the primary energy savings offered by a CHP plant compared with (conventional) separate production of electrical and thermal energy.

The *PES* index is calculated as (European Parliament, 2004):

$$PES = 1 - \frac{1}{\frac{\bar{\eta}_{el}}{\eta_{el\_ref}} + \frac{\bar{\eta}_{th}}{\eta_{th\_ref}}} \tag{4}$$

where:

- $\bar{\eta}_{el}$ and $\bar{\eta}_{th}$ are the electrical and thermal efficiencies of the cogeneration system averaged over a given period; and
- η_{el_ref} and η_{th_ref} are the reference values of efficiency for separate production of electrical and thermal energy.

A positive value of the index means that the primary energy consumption of the CHP system is lower compared with separate production over the time period considered. Figure 9 shows the *PES* index of a Turbec T100 PH in different operating conditions for

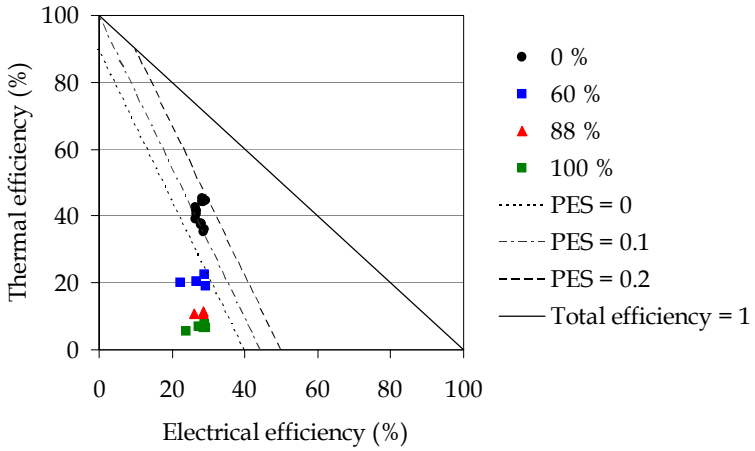

Fig. 9. PES for different degrees of BPV opening

different degrees of BPV opening, calculated considering values of 40 % and 90 % of η_{el_ref} and η_{th_ref}, respectively. It is worth noting that heat recovery is crucial to achieve a positive *PES*. In fact, even minor opening of the BPV adversely affects the index. This confirms that thermal priority operation (0 % BPV opening) is the mode maximizing fuel savings and consequently that it is preferable to the electrical priority mode.

5. Enhancing performances

As noted above, major limitations to the further spread of MGTs are their lower electrical efficiency compared with their main competitors, i.e. reciprocating engines, and lower electrical power production at rising ambient temperatures. Their main advantages, low emissions and competitive O&M costs, do not seem to offset these drawbacks.
In the following paragraphs we describe the research work being conducted by the Systems for Energy and the Environment team of Dipartimento di Energetica, Università Politecnica delle Marche, Ancona, Italy, to enhance MGT performance. We employed the same MGT model that was used to obtain the experimental performance and emissions data, focusing on:

1. Inlet Air Cooling (IAC);
2. Bottoming organic Rankine cycles;
3. Micro STIG;
4. Trigeneration.

5.1 Inlet Air Cooling (IAC)

The simplest way to limit the power reduction consequent to rising ambient temperature is to cool the air entering the compressor.
The air intake system of the MGT studied consists of a single duct carrying the working air and the cooling air, which both enter a single ambient inside the cabinet. From here part of the air is sucked in by the compressor, while the remaining air flow is conveyed to the cooling system via an external fan. Clearly, only the air processed by the compressor influences performance. Hence the need for separating the two flows, in order to cool only the working air. This can be achieved with minimum changes to the MGT cabinet and by mounting a cooling system in the working air inlet duct.
For the MGT model studied ice formation in the air flow and on the walls, a common risk in GTs, is excluded by the manufacturer, who states extreme working condition (-25 °C air temperature, 100 % R.H.) that are much more severe than those that can be achieved with any cooling system.
We used a test bed to evaluate two different IAC techniques:

- direct expansion IAC system;
- fogging IAC system.

The tests were conducted in the summer in the ambient condition of an Adriatic seaside town in central Italy.

Direct expansion IAC system

This system consists of a refrigerating engine, whose evaporator is housed directly in the working air intake duct. The refrigerating engine and the condenser fans are electrically driven by means of inverters, to improve efficiency. The system uses R507A as the refrigerating fluid and is designed to keep the inlet air temperature at the value set by the user, external ambient conditions and refrigerating engine power permitting. In fact,

although an inlet air cooled temperature of 15 °C (ISO, 1989) was set for all the tests, it was not reached consistently. As an example, Figures 10 and 11 show the electrical power and efficiency, respectively, in relation to ambient temperature, R.H., and corresponding IAC temperature over 200 time steps (about 15 min), with the machine working at maximum load. Since the R.H. was greater than the design R.H. (50 %), the minimum IAC temperature that could be achieved was slightly > 15 °C (about 17 °C).

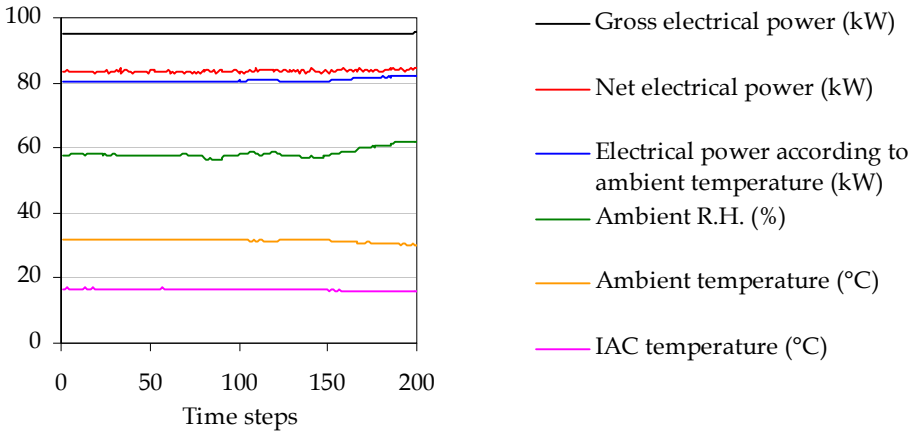

Fig. 10. Effects of the direct expansion IAC system on inlet air and MGT electrical power production

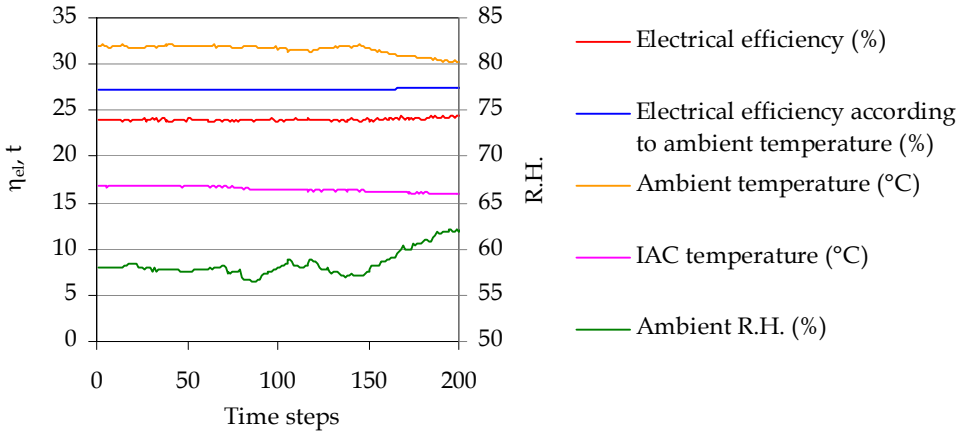

Fig. 11. Effects of the direct expansion IAC system on inlet air and MGT electrical efficiency

The IAC temperature induced a significant increase in gross electrical power production, from about 80 kW (without IAC) to around 95 kW.

However, the net electrical power, which is the crucial output, reached only 84 kW, due to the strong influence of the refrigerating engine performance: the lower its coefficient of

performance (COP), the higher its consumption and the lower the net electrical power of the MGT. The COP thus emerges as a crucial parameter, since an excessively low COP can entail a net electrical power even lower than the one without IAC. The COP measured during these tests was about 2.5. The power increase notwithstanding, the consumption of the refrigerating engine adversely affects the electrical efficiency of the MGT. To sum up, the direct expansion IAC system can be used to increase electrical power, but it does not enhance efficiency.

Fogging IAC system

This system cools the inlet working air via adiabatic saturation (Chaker et al., 2000). The main components of the apparatus are nozzles (4 in our test bed) and a high-pressure pump. Demineralized water is pumped at a pressure of 70 bar to the nozzles, housed in the intake duct, and is then nebulized as droplets whose diameter is usually < 20 μm (Chaker et al., 2002). The fogging system thus achieves nearly total adiabatic saturation by cooling the air to wet bulb temperature, which is the lowest achievable temperature, at an R.H. of about 100 %. For this reason, the final cool air temperature cannot be preset, but is strongly dependent on ambient conditions: the drier the air, the greater the temperature reduction. Figures 12 and 13 show electrical power and efficiency, respectively, over a period of 200 time steps with the machine working at its maximum load. Thanks to the IAC temperature, electrical power production increases from about 84 kW to 88 kW, but unlike in the direct expansion IAC system, here it is very close to the net electrical power, since the high-pressure pump consumes only 550 W. Furthermore, the fogging system slightly improves electrical efficiency, by about 1 %.

In conclusion, both IAC techniques were effective in limiting the electrical power reduction consequent to rising ambient temperature. Despite the comparable power gain, the fogging technique is however preferable, ambient conditions permitting, since besides enhancing efficiency it involves a much simpler and, last but not least, cheaper plant. Expansion techniques would be interesting if the refrigerating engine were also used for other purposes, such as air conditioning of large spaces (e.g. shopping malls, cinemas, office blocks). Since air conditioning plants are designed on the warmest local conditions, they work at partial load most of the time; the residual power could therefore be used for IAC.

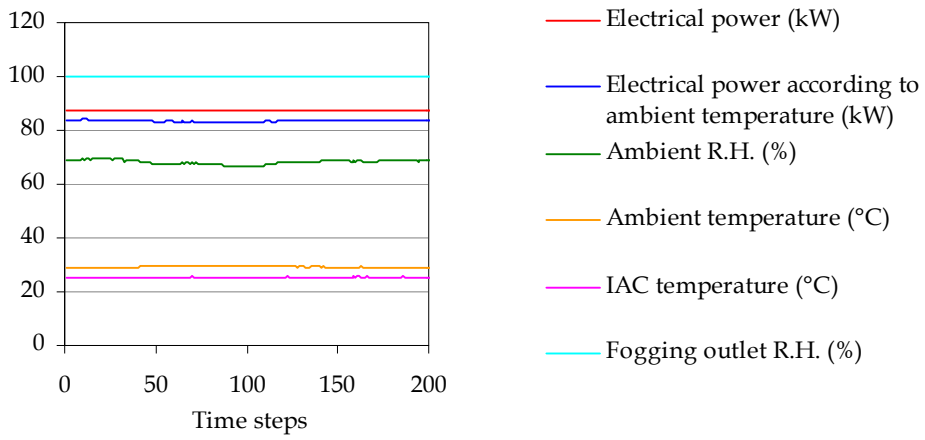

Fig. 12. Effects of the fogging IAC system on inlet air and MGT electrical power production

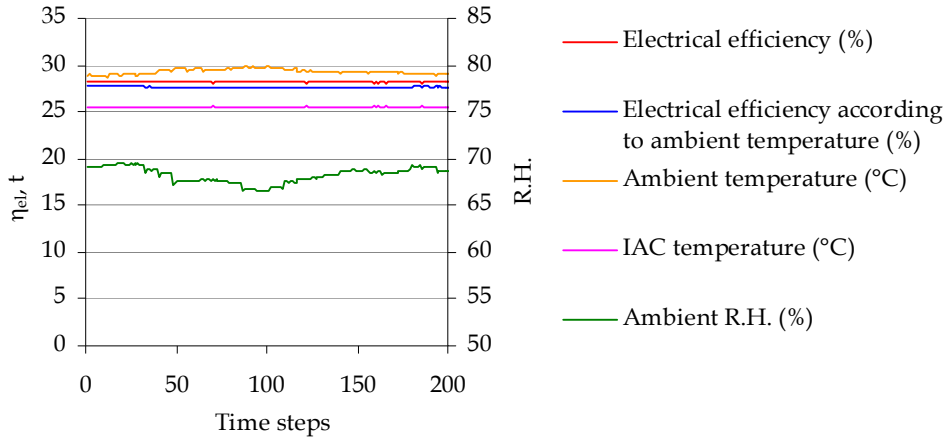

Fig. 13. Effects of the fogging IAC system on inlet air and MGT electrical efficiency

5.2 Bottoming organic Rankine cycles

The solution proposed here aims to enhance the electrical efficiency of the MGT by recovering the heat lost, producing additional electricity. This goal can be achieved with a micro combined cycle using bottoming organic Rankine cycles (Caresana et al., 2008). This micro combined configuration consists of an MGT, a Heat Recovery Vapour Generator (HRVG), and a bottoming vapour plant (Figure 14). This solution minimizes the changes to the standard CHP model, since it merely requires replacing the original HRB with an HRVG. The MGT exhausts enter the HRVG and are discharged to the environment after heating the bottoming working fluid. The vapour generated in the HRVG expands through a turbine that drives an electrical generator.

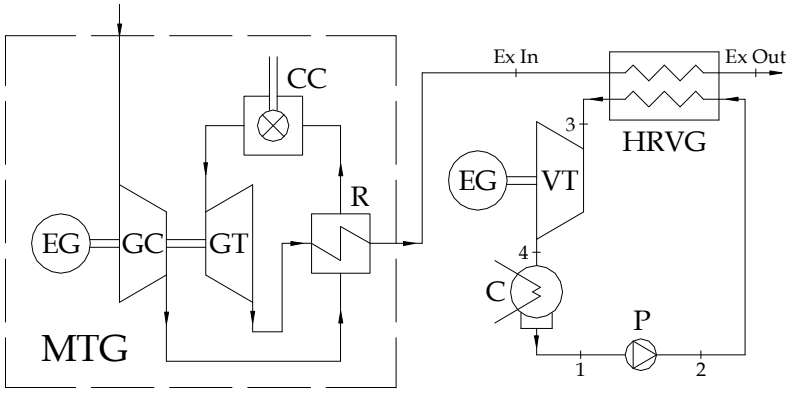

EG	Electrical Generator	GC	Gas Compressor
GT	Gas Turbine	CC	Combustion Chamber
R	Regenerator	C	Condenser
VT	Vapour Turbine	HRVG	Heat Recovery Vapour Generator
P	Pump		

Fig. 14. Layout of the micro combined plant

Clearly, this configuration greatly affects the cogeneration plant's performance, since the thermal energy is discharged at the bottoming cycle condenser at very low temperatures.

Selection of the bottoming cycle working fluid

Whereas traditional, large-size, combined plants commonly use water as the bottoming cycle working fluid, organic fluids seem to be more appropriate in micro scale plants, because their thermodynamic properties are better suited to the low temperature of the exhausts leaving the MGT. Compared with steam, organic fluids allow both more compact solutions, by virtue of their higher density, and simpler layouts, by virtue of their significantly narrower density variation through evaporation and expansion.
This work does not examine some common, technically suitable organic fluids, i.e. chlorofluorocarbons (CFCs), because they have been banned (United Nations, 2000), and hydrochlorofluorocarbons (HCFCs), because they will be banned in the European Union, from January 1st 2015 (European Parliament, 2000). Therefore the choice necessarily falls on hydrofluorocarbons (HFCs) due to thermo-physical and technical criteria. In fact, the fluid in question needs to be:

- thermally stable in the range of pressures and temperatures involved in the cycles;
- non-toxic;
- non-corrosive;
- non-explosive;
- non-flammable;
- compatible with the plant's process component materials;
- low ozone-depleting;
- global warming-neutral.

HFCs meeting these criteria include R245ca, R245fa, R134a, R407C and R410A, the last two being mixtures. Their liquid-vapour curves are reported in a T-s diagram in Figure 15 and their critical properties in Table 1.

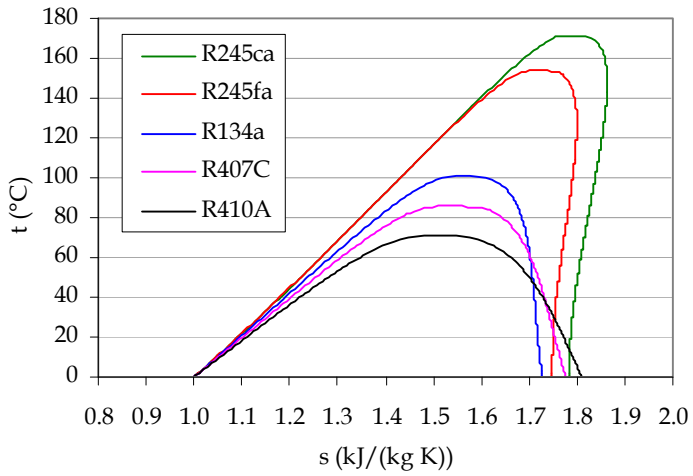

Fig. 15. T-s diagrams of five HFC organic fluids

In particular Figure 15 shows that R245fa and R245ca are "dry fluids", R407C and R410A are "wet fluids", and R134a is an almost "isoentropic fluid". A dry fluid is one whose vapour saturation curve with reference to a given temperature interval has a positive slope on a T-s diagram (dT/dS>0); a wet fluid is one having a negative slope (dT/dS<0), and an isoentropic fluid is a fluid having a vertical saturation line (dT/dS= ∞).

	R245ca	R245fa	R134a	R407C	R410A
Temperature (°C)	174.42	154.05	101.06	86.03	71.36
Pressure (MPa)	3.925	3.640	4.059	4.630	4.903

Table 1. Critical points of the five HFCs

Bottoming cycles

Vapour cycles can be: (i) non-superheated or Rankine type; (ii) superheated or Hirn type; or (iii) supercritical. Steam cycles are commonly superheated, due to thermodynamic efficiency requirements and to the need for limiting droplet condensation during vapour expansion through the turbine. With organic cycles the latter problem is partially addressed by proper selection of the working fluid. Use of a dry fluid prevents droplet condensation in the turbine even without superheating. In fact, at a suitable evaporating pressure the expanding dry fluid does not enter the liquid-vapour equilibrium zone and condensation does not take place, even starting from the saturated vapour line. However, superheating is still a valuable option, since the benefit of removing the superheater must be weighed against the consequent decrease in efficiency. In this subsection we present the results of simulations, performed with an in house-developed program, where different vapour cycle configurations were tested using the five organic fluids mentioned above.
Since the exhaust mass flow rate and outlet temperature of the MGT studied are known, the bottoming cycles can be defined completely by setting the values of the following parameters:

- vapour cycle condensing pressure, p_c ;
- HRVG pressure, p_v ;
- vapour cycle maximum temperature, t_3 .

Furthermore, setting the exhaust temperature at the HRVG outlet, $t_{Ex\ Out}$, allows calculation of the thermal power that can be recovered from the exhausts, P_{t_rec} , as:

$$P_{t\_rec} = \dot{m}_{eg} \cdot c_{p\_eg} \cdot \left(t_{Ex\ In} - t_{Ex\ Out} \right) \tag{5}$$

where $\dot{m}_{eg}$ and c_{p_eg} are the exhaust mass flow rate and its specific heat, respectively. Considering the HRVG as adiabatic, the organic fluid mass flow rate, $\dot{m}_V$, is therefore:

$$\dot{m}_V = \frac{P_{t\_rec}}{q_{in}} \tag{6}$$

where q_{in} is the heat received by the organic fluid unit of mass (see fluid states of Figure 14), which is equal to the increase in enthalpy through the HRVG:

$$q_{in} = h_3 - h_2 \tag{7}$$

The condensing pressure p_c depends closely on the temperature of the cooling fluid at the condenser, t_{cf_in}, and results in a condensing temperature, t_c, of:

$$t_c = t_{cf\_in} + \Delta t_{cf} + \tau \tag{8}$$

where, as shown in Figure 16, Δt_{cf} is the temperature increase of the cooling fluid through the condenser and τ is the temperature difference between the condensing organic fluid and the cooling fluid at the outlet.

The values of τ and Δt_{cf} are the result of a technical and economic trade-off. The lower these values, the lower the condensing temperature and the greater the cycle's efficiency, as well as the heat exchanger's surface and cost. The study considers four condensing technologies, of which the water-cooled system is the most appropriate. However, it also addresses cooling technologies that reduce the amount of water needed, such as cooling towers, or that completely obviate the need for it, such as air condensers for use at sites where water is not consistently available. Finally, it examines condensation with water coming from a panel heating system, which makes the plant a micro combined cogeneration system. The condensing technologies considered, the assumed values of t_{cf_in}, Δt_{cf}, τ and the resulting t_c and p_c are reported in Table 2.

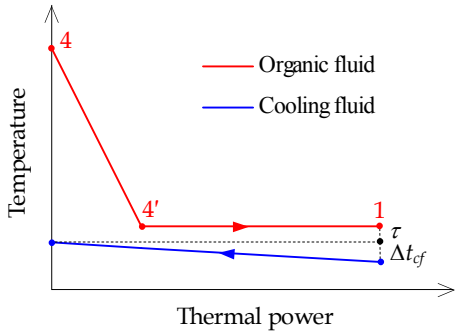

Fig. 16. Condenser heat exchange diagram

Condensing technology	t_{cf_in} (°C)	Δt_{cf} (°C)	τ (°C)	t_c (°C)
Condenser cooled by ambient air	15	8	7	30
Condenser cooled by ambient water	12	8	7	27
Condenser cooled by water from cooling tower	15	8	7	30
Condenser cooled by water from panel heating	30	5	7	42

Table 2. Main parameters of the condensing technologies

An air temperature of 15 °C and an R.H. of 60 % are assumed for condensers cooled by ambient air and by water from a cooling tower, according to the ambient ISO conditions considered for the gas cycle. In particular, the temperature of the water from the cooling

tower is assumed to be 4 °C warmer than the wet bulb temperature of the air, which is about 11 °C in ISO conditions. For the water cooled condenser, the ambient water temperature is assumed to be 12 °C. Finally, if the heat discharged by the vapour cycle is recovered in a panel heating plant, it is considered to require water at 35 °C, which then returns to the condenser at 30 °C.

Once p_c has been calculated, all relevant plant parameters can then be obtained using the set of equations listed in Table 3, where the indexes refer to the points in Figures 14-22 and the assumed efficiencies are listed in Table 4.

The efficiency of the combined plant was then optimized for Rankine, Hirn and supercritical bottoming cycles using this set of equations (eqs. 5-18).

For each condensing pressure, the optimization process involved identification of the combination of p_v and t_3 maximizing the efficiency of the combined plant and meeting the following conditions:

1. minimum vapour quality at the turbine outlet equal to 0.9;
2. minimum temperature difference, $\tau_{\min}$, of 15 °C between the exhausts and the organic fluid inside the HRVG.

The heat exchange and T-s diagrams of the different cycle configurations examined are reported in Figures 17-22.

Vapour cycle output heat per unit of mass	$q_{out} = h_4 - h_1$	(9)
Vapour cycle expansion work per unit of mass	$l_{turbine} = h_3 - h_4 = (h_3 - h_{4is}) \cdot \eta_{turbine}$	(10)
Vapour cycle pumping work per unit of mass	$l_{pump} = h_2 - h_1 = \frac{h_{2is} - h_1}{\eta_{pump}}$	(11)
Vapour cycle thermodynamic efficiency	$\eta = \frac{l_{turbine} - l_{pump}}{q_{in}}$	(12)
Vapour cycle electrical power	$P_{el\_V} = \left[\left(l_{turbine} \cdot \eta_{m\_t} \cdot \eta_{el\_g} \right) - \left(\frac{l_{pump}}{\eta_{m\_p} \cdot \eta_{el\_p}} \right) \right] \cdot \dot{m}_v \cdot \eta_{aux}$	(13)
Combined plant electrical power	$P_{el\_CC} = P_{el} + P_{el\_V}$	(14)
Combined plant electrical efficiency	$\eta_{el\_CC} = \frac{P_{el\_CC}}{\dot{m}_f \cdot LHV}$	(15)
Vapour cycle thermal power output	$P_{th\_CC} = \dot{m}_V \cdot q_{out}$	(16)
Combined plant thermal efficiency (panel heating system)	$\eta_{th\_CC} = \frac{P_{th\_CC}}{\dot{m}_f \cdot LHV}$	(17)
Combined plant global efficiency (panel heating system)	$\eta_{g\_CC} = \frac{P_{el\_CC} + P_{th\_CC}}{\dot{m}_f \cdot LHV}$	(18)

Table 3. Equations used to define the main parameters of the combined plant

Turbine efficiency	$\eta_{turbine}$	0.75
Turbine mechanical efficiency	η_{m_t}	0.98
Electrical generator efficiency	η_{el_g}	0.97
Pump efficiency	η_{pump}	0.70
Pump mechanical efficiency	η_{m_p}	0.98
Pump motor electrical efficiency	η_{el_p}	0.92
Auxiliary system efficiency (water-cooled condenser and panel heating system) *	η_{aux}	0.90
Auxiliary system efficiency (air condenser and cooling tower)*	η_{aux}	0.80
* The power used by fan coils is assumed to reduce the auxiliary system efficiency of the air-cooled condenser and of the cooling tower		

Table 4. Efficiency values assumed for the calculations

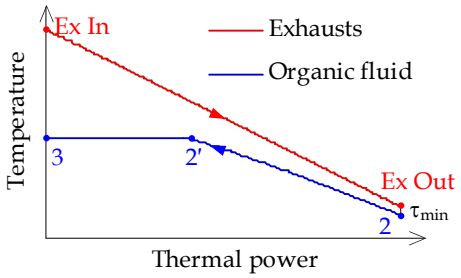

Fig. 17. Rankine cycle heat exchange diagram

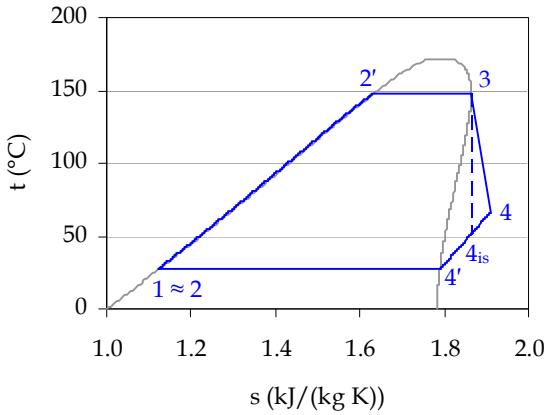

Fig. 18. Rankine cycle

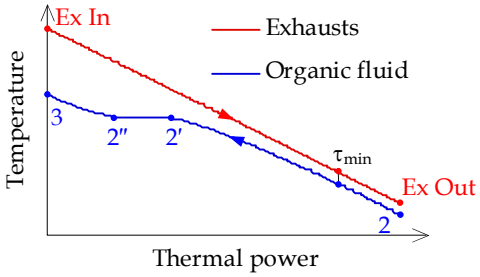

Fig. 19. Hirn cycle heat exchange diagram

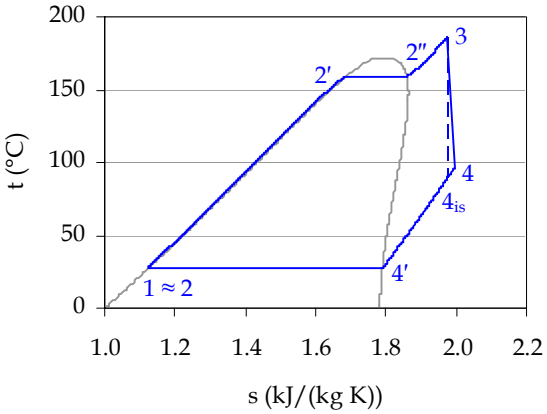

Fig. 20. Hirn cycle

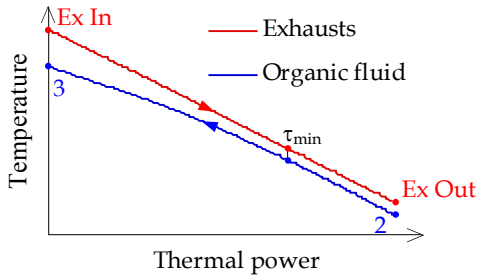

Fig. 21. Supercritical cycle heat exchange diagram

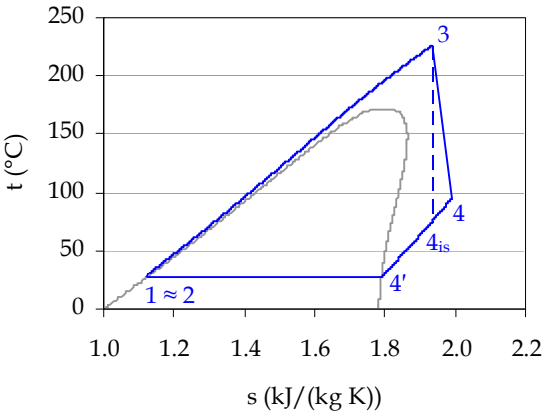

Fig. 22. Supercritical cycle

Performance and results

As expected, the optimization process highlighted that the ambient water condensing technology maximizes the power production of all bottoming cycle configurations with all the organic fluids studied, thus also maximizing both the power production and the electrical efficiency of the whole micro combined plant. The main results of the optimization processes for the ambient water condenser are reported for illustrative purposes in Table 5, where the operating data of each cycle configuration and organic fluid are compared. Only the dry fluids R245 ca and R245 fa are entered for the Rankine cycle. For the Hirn cycle the evaporating pressure is clearly lower than the critical one.

Table 5 shows the organic fluids R245ca and R245fa to be those offering the best performance, with slightly better results for the former. Even though these fluids can be employed in Rankine cycles, achieving an electrical efficiency of 36 - 37 %, compared with the original 30 % of the MGT, better results are achieved with the Hirn (37 %) and, especially, the supercritical cycle (37 - 38 %). The performances of the latter cycles are slightly better than that of the Rankine cycle, but they are based on significantly higher values of HRVG pressure and of t_3. The Rankine bottoming cycle therefore remains a good option, due to the lower pressure and temperature levels and to the simpler plant configuration.

The results of the optimization process of the ambient water condenser with R245fa supercritical cycles are shown in Figure 23, where the electrical power produced by the bottoming cycle is plotted as a function of the evaporating pressure and is parameterized with reference to the t_3.

The electrical power that can be achieved based on t_c with R245ca supercritical cycles as a function of the evaporating pressure is reported in Figure 24 with reference to the water cooling technology. These data are also representative of the other condensing technologies, the only difference being the efficiency of the auxiliary system.

Supercritical							
Working fluid	p_v (MPa)	t_v (°C)	η (%)	$\dot{m}_v$ (kg/s)	P_{el_V} (kW)	P_{el_CC} (kW)	η_{el_CC} (%)
R245ca	7.82	226	17.11	0.577	26.57	126.57	38.01
R245fa	8.92	226	16.51	0.594	25.66	125.66	37.74
R134a	8.25	181	13.71	0.702	21.13	121.13	36.38
R407C	8.33	161	11.78	0.736	17.89	117.89	35.40
R410A	9.65	160	11.74	0.716	17.66	117.66	35.33

Hirn							
Working fluid	p_v (MPa)	t_v (°C)	η (%)	$\dot{m}_v$ (kg/s)	P_{el_V} (kW)	P_{el_CC} (kW)	η_{el_CC} (%)
R245ca	3.72	186	16.24	0.586	25.37	125.37	37.65
R245fa	3.63	183	15.15	0.598	23.68	123.68	37.14
R134a	4.05	180	11.54	0.604	17.94	117.94	35.42
R407C	4.33	162	9.34	0.630	14.47	114.47	34.38
R410A	4.60	162	8.36	0.601	12.93	112.93	33.91

Rankine							
Working fluid	p_v (MPa)	t_v (°C)	η (%)	$\dot{m}_v$ (kg/s)	P_{el_V} (kW)	P_{el_CC} (kW)	η_{el_CC} (%)
R245ca	2.45	148	15.10	0.658	23.62	123.62	37.12
R245fa	2.31	129	13.66	0.728	21.32	121.32	36.43

Table 5. Condenser cooled by ambient water (t_c = 27 °C)

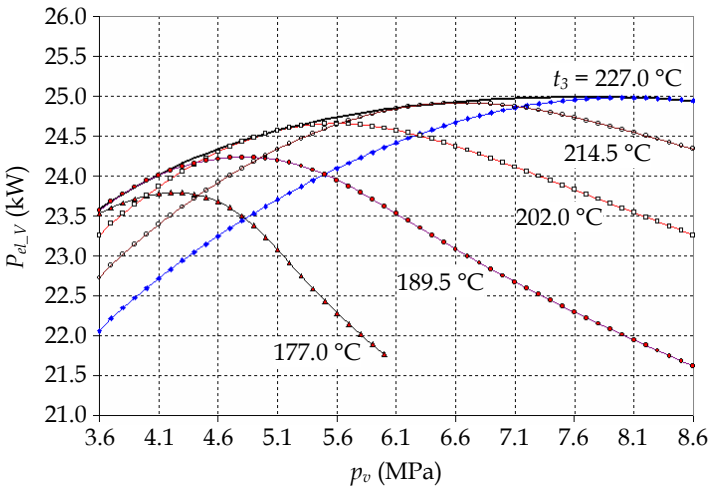

Fig. 23. P_{el_V} as a function of p_v and t_3 for an R245fa supercritical cycle at t_c = 27 °C

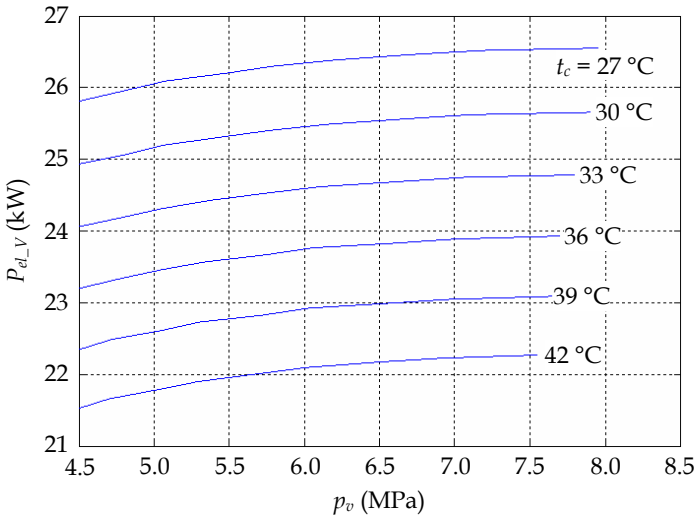

Fig. 24. P_{el_V} as a function of p_v and t_c for an R245ca supercritical cycle

Figure 24 confirms that the lower the condensing pressure, the more the electrical power generated; this applies to all the organic fluids studied. Nevertheless, despite the influence of the high condensing temperature on electrical performances, the cogeneration solution with the panel heating system results in increased global efficiency due to heat recovery.

5.3 Micro STIG

The acronym STIG stands for "Steam-Injected Gas" turbines, a technique used to improve the electrical and environmental performance of large-size GTs. The enhanced electrical power production and system efficiency are related to the different composition and quantity of the working fluid mass flowing through the turbine, due to the steam injected into the combustion chamber zone. The steam also involves a reduction in the combustion temperature and therefore of the NO_x formed in the exhausts.

Our group has recently addressed the advantages of applying the well-known STIG technique to MGTs, from a theoretical standpoint.

In the micro STIG plant layout reported in Figure 25 the original HRB is replaced with a heat recovery steam generator (HRSG), which produces the steam to be injected into the combustion chamber.

The aim was to devise a mathematical model of the micro STIG plant. Each component was defined by a set of equations describing its mass and energy balances and its operating characteristics, the most significant of which are the performance curves of the turbomachines.

The model was used to assess the influence of steam mass flow rate on electrical power and efficiency. Figures 26 to 28 report examples of the preliminary results obtained with the model. In particular, Figures 26 and 27 show electrical power and efficiency, respectively, as a function of the injected steam mass flow rate in fixed thermodynamic conditions (10 bar and 280 °C). Figure 28 shows, for a given flow rate (50 g/s), the trend of the electrical efficiency as a function of steam pressure and temperature.

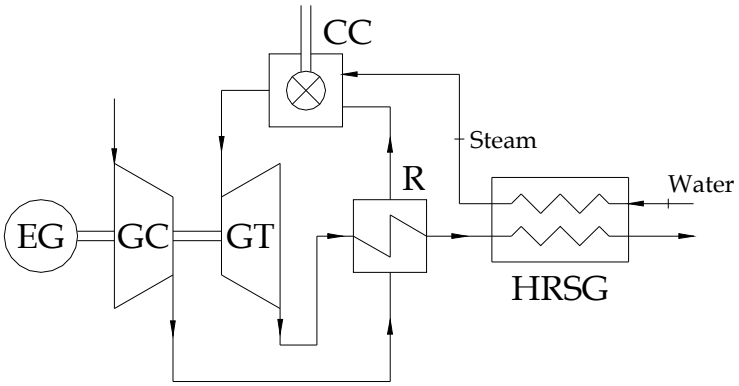

EG	Electrical Generator	GC	Gas Compressor
GT	Gas Turbine	CC	Combustion Chamber
R	Regenerator	HRSG	Heat Recovery Steam Generator

Fig. 25. Layout of the STIG cycle-based micro gas turbine

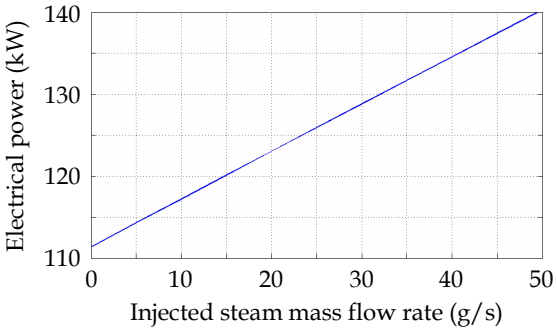

Fig. 26. Electrical power vs. injected steam mass flow rate

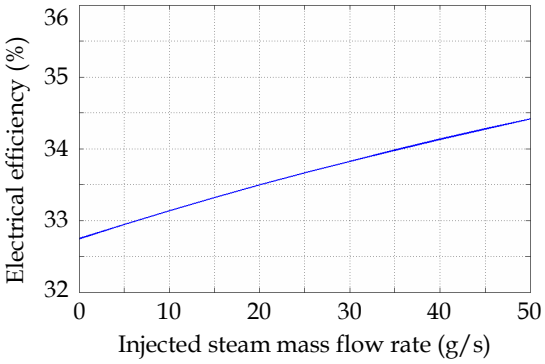

Fig. 27. Electrical efficiency vs. injected steam mass flow rate

Preliminary simulations showed that the more steam is injected the greater are electrical power and efficiency. Nevertheless, the amount of steam that can be injected is affected on the one hand by the thermal exchange conditions at the HRSG—which limit its production—and on the other by the turbine choke line, which limits the working mass flow rate.
Once the amount of steam to be injected has been set, the higher its temperature and pressure, the greater the electrical efficiency.

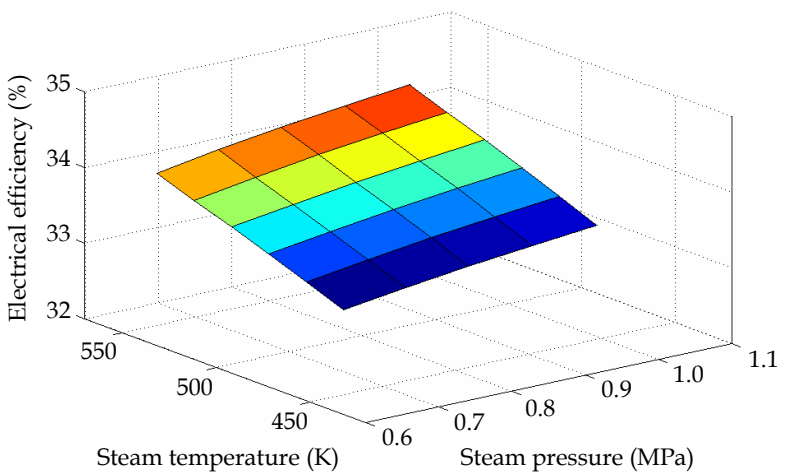

Fig. 28. Electrical efficiency vs. injected steam thermodynamic state

We are currently conducting a sensitivity analysis to assess the thermodynamic state and the amount of injected steam that will optimize the performance of the STIG cycle.

5.4 Trigeneration

The issue of heat recovery has been addressed in paragraph 4.2. Cogeneration systems are characterized by the fact that whereas in the cold season the heat discharged by the MGT can be recovered for heating, there are fewer applications enabling useful heat recovery in the warm season. In fact, apart from industrial processes requiring thermal energy throughout the year, cogeneration applications that include heating do not work continuously, especially in areas with a short winter. The recent development of absorption chillers allows production of cooling power for air conditioning or other applications. This configuration, where the same plant can simultaneously produce electrical, thermal and cooling power, is called trigeneration. The main components of an actual trigeneration plant, designed by our research group for an office block, is shown in Figure 29. The plant, whose data acquisition apparatus is still being developed, consists of a 100 kWe MGT (right) coupled to a heat recovery boiler (centre) and to a 110 kWf absorption chiller (left). The exhausts can be conveyed to the boiler or to the chiller, the latter being a direct exhausts model.

Fig. 29. Trigeneration plant

6. Conclusions

This overview of the state of the art of MGTs has highlighted the critical function of heat recovery in enhancing the energy competitiveness of the technology. Cogeneration or trigeneration must therefore be viewed as native applications of MGTs. The main limitations of the MGT technology are the high sensitivity of electrical power production to ambient temperature and electrical efficiency. The dependence on ambient temperature can be mitigated by using IAC techniques; in particular, the fogging system was seen to be preferable under all respects to an ad hoc-designed direct expansion plant.
Two options have been analysed to increase electrical efficiency: organic Rankine cycles and a STIG configuration. The former technology is easier to apply, since it does not require design changes to the MGT, but merely replacement of the recovery boiler with an organic vapour generator. Furthermore, the technology is already available on the market, since it has already been developed for other low-temperature heat recovery applications.
In contrast, the STIG configuration requires complete redesign of the combustion chamber, as well as revision of both the control system and the housing. Both technologies enhance electrical efficiency to the detriment of global efficiency, since both discharge heat at lower temperature, so that cogeneration applications are often not feasible.

7. Acknowledgements

This work was supported by the Italian Environment Ministry and by the Marche Regional Government (Ancona, Italy) within the framework of the project "Ricerche energetico-ambientali per l'AERCA di Ancona, Falconara e bassa valle dell'Esino".
Thanks to Dr. Silvia Modena for the language review.

8. References

Caresana, F.; Pelagalli, L., Comodi, G. & Vagni, S. (2006); Banco prova per la verifica delle prestazioni di una microturbina a gas ad uso cogenerativo, *Atti della Giornata Nazionale di Studio MIS-MAC IX, Metodi di Sperimentazione nelle Macchine,* pp. 207-218, ISBN: 88-89884-02-9, Trieste, March 2006

Caresana, F.; Pelagalli, L., Comodi, G. & Vagni, S. (2008); Micro combined plant with gas turbine and organic cycle, *Proceedings of the ASME Turbo Expo 2008,* Volume 1, pp. 787-795, ISBN: 978-0-7918-4311-6, Berlin, May 2008

Chaker, M.; Meher-Homji, C. B. & Mee III, T. R. (2000) Inlet fogging of gas turbine engines - Part A: Theory, psychrometrics and fog generation, *Proceedings of ASME Turbo Expo 2000*; pp. 413-428, Volume 4 A, Munich, May 2000

Chaker, M.; Meher-Homji, C. B., Mee III, T. (2002) Inlet fogging of gas turbine engines - Part B: Fog droplet sizing analysis, nozzle types, measurement and testing, *Proceedings of the ASME Turbo Expo 2002*; Volume 4 A, 2002, pages 429-441, Amsterdam, June 2002

European Parliament (2000). Regulation (EC) No 2037/2000 of the European Parliament and of the Council of 29 June 2000 on substances that deplete the ozone layer

European Parliament (2004). Directive 2004/8/EC of the European Parliament and of the Council of 11 February 2004 on the promotion of cogeneration based on a useful heat demand in the internal energy market and amending Directive 92/42/EEC

GTW (2009) - *Gas Turbine World Handbook 2009* – Volume 27

IEA (2002), International Energy Agency. *Distributed generation in liberalised electricity markets*. http://www.iea.org/textbase/nppdf/free/2000/distributed2002.pdf, OECD/IEA 2002

ISO (1989). ISO 2314: 1989, "Gas turbines - Acceptance tests"

Macchi E.; Campanari, S. & Silva, P. (2005). *La Microcogenerazione a gas naturale*. Polipress ISBN 8873980163 Milano.

Pepermans G.; Driesen J., Haeseldonckx, D., Belmans R. & D'haeseleer, W. (2005). Distributed generation: definition, benefits and issues, *Energy Policy*, 33 (2005), pp. 787–798, ISSN 0301-4215

Turbec (2002)."Technical description", D12451, Turbec AB, 17 June 2002

United Nations (2000). United Nations Environment Programme, Secretariat for The Vienna Convention for the Protection of the Ozone Layer & The Montreal Protocol on Substances that Deplete the Ozone Layer, "Montréal Protocol on Substances that Deplete the Ozone Layer as either adjusted and/or amended in London 1990 Copenhagen 1992 Vienna 1995 Montreal 1997 Beijing 1999", March 2000

Zogg, R.; Bowman, J., Roth, K. & Brodrick, J. (2007). Using MGTs for distributed generation. *ASHRAE Journal,* 49 (4), pp. 48-51 (2007), ISSN 0001-2491.

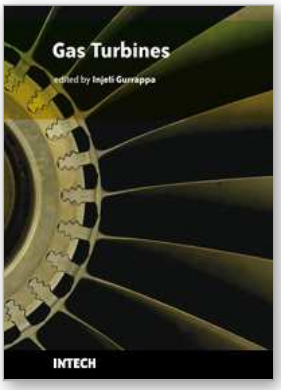

Gas Turbines

Edited by Gurrappa Injeti

ISBN 978-953-307-146-6
Hard cover, 364 pages
Publisher Sciyo
Published online 27, September, 2010
Published in print edition September, 2010

This book is intended to provide valuable information for the analysis and design of various gas turbine engines for different applications. The target audience for this book is design, maintenance, materials, aerospace and mechanical engineers. The design and maintenance engineers in the gas turbine and aircraft industry will benefit immensely from the integration and system discussions in the book. The chapters are of high relevance and interest to manufacturers, researchers and academicians as well.

InTech Europe
University Campus STeP Ri
Slavka Krautzeka 83/A
51000 Rijeka, Croatia
Phone: +385 (51) 770 447
Fax: +385 (51) 686 166
www.intechopen.com

InTech China
Unit 405, Office Block, Hotel Equatorial Shanghai
No.65, Yan An Road (West), Shanghai, 200040, China
中国上海市延安西路65号上海国际贵都大饭店办公楼405单元
Phone: +86-21-62489820
Fax: +86-21-62489821